Available online at www.sciencedirect.com

SciVerse ScienceDirect

journal homepage: www.elsevier.com/locate/he

Operando infrared spectroscopy of the fuel cell membrane electrode assembly Nafion–platinum interface

*Ian Kendrick, Eugene S. Smotkin**

Department of Chemistry and Chemical Biology, Northeastern University, Boston, MA 02115, USA

ARTICLE INFO

Article history:
Received 18 May 2013
Received in revised form
22 July 2013
Accepted 29 July 2013
Available online 28 August 2013

Keywords:
Nafion
Fuel cell
Operando infrared spectroscopy
Platinum

ABSTRACT

The Nafion–Pt interfaces in membrane electrode assemblies of operating fuel cells were studied by operando infrared spectroscopy. The potential dependence of atop adsorbed CO peak frequencies were measured over the potential range of 0–600 mV (vs. NHE) at 60 °C. Complex Stark tuning of peak frequencies arise from a combination of potential dependent coverage effects, and changes in the extent of back-donation from the metal d-band to the renormalized $2\pi^*$ MO of CO_{ads}. The Nafion–Pt interface was studied at higher potentials (initiating at open circuit) by examining platinum reflectivity as a function of electrode potential. The oxygen reduction onset-current is coincident with the observance of a 2% step-increase in Pt reflectivity and emergence of Nafion–Pt interface spectra.

1. Introduction

The ionomer-catalyst interface is the site of chemical transformation in a polymer electrolyte fuel cell membrane electrode assembly (MEA). The MEA is a polymer electrolyte membrane sandwiched between anode and cathode catalytic layers. The electrocatalytic layers are contacted to porous carbon paper or cloth that serve both as current collectors and gas diffusion layers (GDLs). The GDLs facilitate transport of reactants and products between the fuel cell flow fields and the ionomer-catalyst interfaces. Catalysts are dispersed in alcoholic solutions of a solubilized version of the polymer electrolyte to form an ink that is deposited on the membrane directly (catalyst-coated-membrane), or deposited directly onto the GDL to form a gas diffusion electrode. The final form of the electrocatalytic layers have carbon supported metal or metal-black surfaces [1] wetted by the ionomer electrolyte. The ionomer facilitates proton transport and enhances electrocatalysis [2].

MEAs have applications in organic synthesis [3–10], environmental remediation [11,12] energy conversion [13] and storage devices [14–17]. Each application requires an ionomer-catalyst interface that is optimized for the required chemical reaction. Optimization requires methods for characterization under *relevant* conditions. Because the active state of the ionomer-catalyst interface exists only during electrocatalysis [18], characterization is best done at normal operating temperatures with typical reactant stream flow (*i.e.*, Operando). Operando methods preclude the use of supplemental electrolytes (e.g., H_2SO_4 or $HClO_4$) that contribute mobile anion adsorbates and dehydrate at the high end of relevant temperatures (e.g. 70–90 °C). Infrared (IR) spectroscopy, ideally suited for the characterization of ionomer-catalyst interfaces, elucidates potential and temperature

* *Corresponding author*. Tel.: +1 617 373 7526.
E-mail address: e.smotkin@neu.edu (E.S. Smotkin).
0360-3199/$ – see front matter
http://dx.doi.org/10.1016/j.ijhydene.2013.07.117

dependent reaction intermediates and competitive adsorbates [19–22]. Such information is required for optimization of ionomer-catalyst interfaces for rapidly emerging applications.

We introduced operando IR spectroscopy of fuel cells [23] for study of mechanistic methanol electro-oxidation on Pt and Pt alloys as well as X-ray absorption spectroscopy of the active phases of alloy catalysts in hydrogen–air [24] and direct methanol fuel cells [25]. More recently we applied operando IR spectroscopy to Nafion–Pt interfaces to better understand the self-assembly of Nafion onto metal surfaces [26–28]. This work focuses on operando spectroscopy of the Nafion–Pt interface in fuel cell MEAs.

2. Experimental

2.1. Membrane electrode assembly preparation

As received Nafion 117 is immersed in boiling 8 M HNO_3 (20 min), rinsed with Nanopure™ water and then immersed in boiling water (20 min). Catalyst inks are prepared by the method of Wilson [29]. Briefly, Pt black (Johnson Matthey) and 5 wt.% Nafion ionomer solution (Sigma Aldrich, Milwaukee, WI) are dispersed in Nanopure™ water. Catalyst coated membranes (CCMs) are prepared by brush painting (Red Sable marking brush size #1, Tanis Inc., Delafield, WI) the ink on 5 cm^2 of Nafion immobilized on a heated vacuum table (NuVant Systems, Crown Point, IN) at 70 °C. The CCM is sandwiched between sheets of carbon paper gas diffusion layers (Toray Industries, Tokyo, Japan) and then installed into the operando spectroscopy fuel cell. The catalyst loadings at both electrodes are 4 mg/cm^2 of Pt black. MEAs were conditioned in the fuel cell at 50 °C by scanning the potential (5 cycles) between 800 mV and 600 mV (40 mV/min) with humidified hydrogen (50 sccm) and air (200 sccm), both at ~0 gauge pressure, delivered to the anode and cathode, respectively. The working electrode is conditioned immediately before obtaining reference spectra by cycling the potential from 0 V to 1.2 V at 100 mV/s, 50 times in the presence of humidified N_2 (200 sccm).

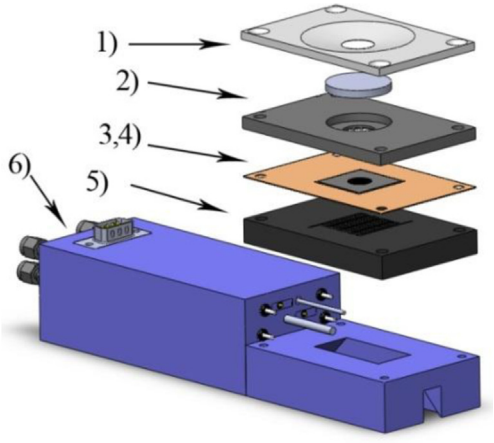

Fig. 1 – Exploded diagram of the IR-XAS cell and components: 1) Top plate, 2) Top flow field, 3) Membrane electrode assembly gasket, 4) Membrane electrode assembly, 5) Lower flow field, and 6) Slider housing.

2.2. Operando spectroscopy

Reflectance IR spectra were obtained using the cell described by Lewis and coworkers (Fig. 1) [27]. The cell is interfaced to a diffuse reflectance stage (Pike Technologies, Madison, WI) and installed in a Vertex 70 spectrometer (Bruker, Billerica, MA). The IR beam accesses the MEA catalytic layer through a CaF_2 window inserted into the upper flow field via a slit cut into the gas diffusion layer. The cell (50 °C) is fed humidified H_2 (50 sccm) and N_2 (200 sccm) to the counter/reference and working electrodes, respectively. After obtaining a reference spectrum at 1.2 V, spectra were acquired from 1.2 V to 0 V at decreasing 0.1 V increments. Spectra were obtained by averaging 100 scans at 4 cm^{-1} resolution using a liquid N_2 cooled MCT detector[1]. Operando interferogram amplitudes were obtained after acquiring each potential dependent FTIR spectra using the Opus 6.5 (Bruker).

Potential dependent IR spectra of linear bound CO (CO_{ads}) were obtained at 60 °C. The small CO oxidation currents do not measurably polarize the counter electrode which is also used as a hydrogen reference electrode [30]. The reference spectrum was acquired at 0 mV. At 300 mV the working electrode feed was switched to CO (40 sccm) for 15 min prior to purging the working electrode with N_2 (15 min). Four signal-averaged (250 scans) spectra were acquired at 100 mV and at increasing 50 mV increments, until the CO vibrational bands were no longer observable. Spectra were obtained at resolution of 4 cm^{-1} using a DLaTGS detector.

3. Results and discussion

Fig. 2 (left) shows the potential dependent spectra of CO_{ads} at the Nafion–Pt interface with the fuel cell at 60 °C. The corresponding Stark tuning curve of $\bar{\upsilon}_{CO}$ vs. potential (Fig. 2 right) is similar to previously reported curves on arc-melted [31] and Pt(111) [32] exposed to 0.5 M H_2SO_4, and on Nafion–platinum interfaces of operating MEAs [23,26,33,34]. Anderson explained Stark tuning in terms of metal-to-adsorbate orbital overlap (*i.e.*, Blyholder mechanism) [35], first with cyanide on Ag [36] and later CO_{ads} on Pt [37]. Norskov provides a detailed description of the π bonding of CO to Pt in two steps [38,39]. In the first step, the $2\pi^*$ and the 5σ CO MOs shift to lower energy and broaden due to coupling with the Pt s,p electrons. The renormalized CO orbitals then mix with the Pt d-band bonding orbitals resulting in the splitting of the $2\pi^*$ MOs into antibonding and bonding orbitals. Thus, a shift of the surface d-band center to more positive potentials decreases the overlap between the surface d-band and the renormalized $2\pi^*$ CO MOs, increasing the carbon–oxygen bond order, and thus increasing the $\bar{\upsilon}_{CO}$. An alternative explanation has been provided by Dimakis et al. [40–44]. Cluster and periodic DFT calculations for CO_{ads} on Pt of pure Pt and Pt-based alloys show that shifts in the binding of the CO to the Pt surface are primarily due to changes in the charges and polarizations of the σ and π metal–CO hybrid

[1] The wavelength precision of an FTIR is determined by the stability of the reference HeNe laser. Virtually all FTIR spectrometers manufactured today are capable of 0.1 cm^{-1} or better precision on the wavelength axis.

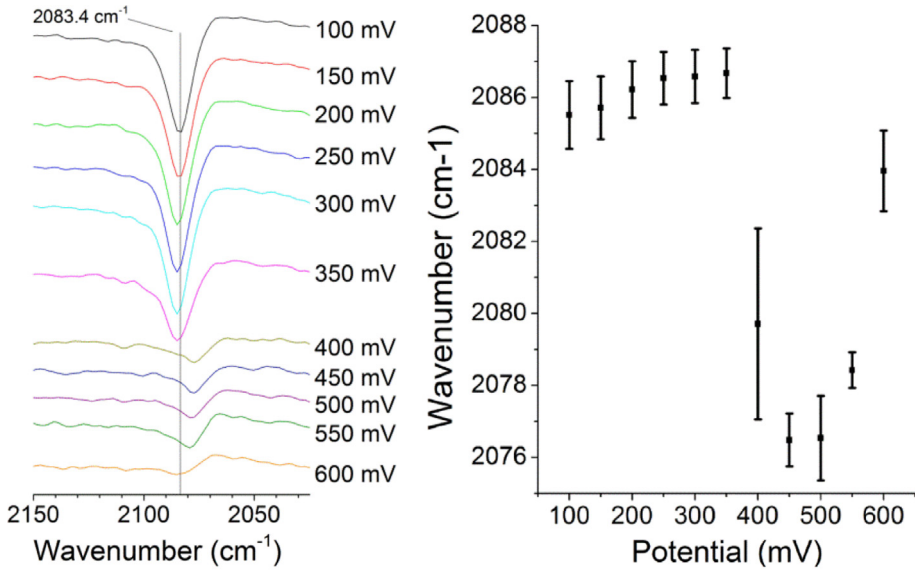

Fig. 2 – Stark tuning of CO adsorbed on a Pt membrane electrode of a fuel cell operating at 60 °C. Left: Potential-dependent IR spectra of CO_{ads} at the Nafion–Pt interface at 60 °C. Right: Stark tuning curve corresponding to potential dependent spectra.

orbitals. The Dimakis approach is consistent with observations of reduced CO_{ads} (atop on Pt) stretching frequencies as Pt is alloyed with Ru [31].

This primary Stark tuning effect explains the positive Stark tuning rate $d\bar{\nu}_{CO}/dE$ initiating at 100 mV (Fig. 2 right). The $d\bar{\nu}_{CO}/dE$ of ~5.4 cm^{-1}/V is typical for MEA incorporated Pt catalysts [26,27,33]. It is important to note that Stark tuning rates (STR) are not simply a property of the adsorbate-substrate identity. Liu et al. reported a comprehensive study of CO_{ads} STRs vs. coverage, Pt alloy composition, potential and temperature [31]. The STRs are strongly affected by secondary effects due to co-adsorbates, adsorbate coverage, and particle size [45]. Stamenkovic [32], followed by Kendrick [26] discussed a very subtle $\bar{\nu}_{CO}$ blue shift from the extrapolated linear region of tuning curves initiated at potentials negative of CO oxidation [32]. The three $\bar{\nu}_{CO}$ points collected from 200 to 300 mV (Fig. 2 right) exemplify this blue shift, which we attribute, in this work, to CO_{ads} island compression due to repulsive dipole interactions with co-adsorbed Nafion sulfonate ion. CO_{ads} oxidation initiating at 0.35 V, induced by co-adsorption of OH^-, diminishes dipole–dipole coupling [46] and thus precipitously decreases $\bar{\nu}_{CO}$. The upturn is attributed to increased adsorption of the Nafion sulfonate exchange sites relative to OH^-, which reestablishes repulsive dipole interactions that compress CO_{ads} islands and increases $\bar{\nu}_{CO}$. The STR plot elucidates adsorption phenomena at the Nafion–Pt interface in the absence of mobile ions typical of dilute sulfuric acid solutions. A detailed model for self-assembly of Nafion onto Pt has been reported [26]. CO_{ads} STR curves are an excellent tool for study of Pt surfaces at low potentials, where CO_{ads} exists at

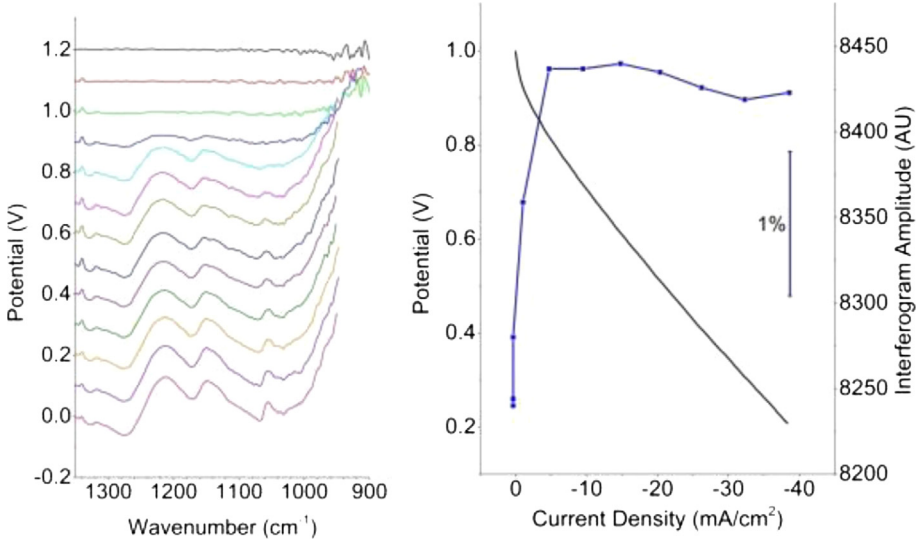

Fig. 3 – Left: Potential dependent spectra of Nafion on Pt under nitrogen. Right: The interferogram amplitude as a function of potential superimposed over a polarization curve obtained with the operando fuel cell under oxygen.

steady state. Higher potentials relevant to Nafion–Pt interfaces operating at the cathode require an alternate method of study because static CO_{ads} are not stable at high potentials. Fan et al. showed that in flowing streams of CO, CO_{ads} can be observed at potentials throughout the entire operating potential range of the fuel cell [23,33].

The operando spectra of the MEA Nafion–Pt interface from 1.2 V to 0 V vs. the hydrogen anode are shown (Fig. 3, left). The corresponding fuel cell current–potential curve, superimposed upon the potential dependent interferogram amplitudes, are shown (Fig. 3, right). An interferogram is an oscillatory series of constructive and destructive combinations of radiation generated by the recombination of light reflected from the moving and fixed mirror of the Michelson interferometer. This radiation is passed through the sample to the detector to generate an IR spectrum [47]. Because the IR technique employed in this study is diffuse reflection, an increase in the reflectivity of the surface would be associated with increased interferogram amplitude. At potentials where Pt is passivated with an oxide layer (1.2 V–1 V vs. hydrogen anode) there is no change in the spectra. At the oxygen reduction onset-current there is a 2% step-increase in Pt reflectivity coincident with the emergence of the full IR reflectance spectrum of Nafion. The step-change in reflectivity is coincident with exposure oxide-free Pt to reactant oxygen. The reflectivity is at maximum just after the current onset and then slightly diminishes with decreasing potential. It is noteworthy that only a 2% change in reflectivity is responsible for the emergence of the Nafion IR reflection spectra. The peak at ~1060 cm^{-1} (Nafion side chain group mode) [48,49] and the broad envelope region (1100–1300 cm^{-1}) rapidly emerge and persist as the potential is reduced. Thus oxygen reduction initiates with the emergence of Nafion–Pt reflectance spectra concurrent with exposure of an oxide free, more reflective Pt surface.

4. Conclusions

The operando spectroscopy of the Nafion–Pt interface in a hydrogen–air fuel cell membrane electrode assembly was used to study Stark tuning rates of CO_{ads}. The Stark tuning of CO_{ads}, at 60 °C, elucidate a complex sequence of co-adsorption as the potential is shifted for CO_{ads} stripping. Nafion co-adsorption is invoked since there are no mobile anions under operando conditions. At higher potentials an increase in the reflectivity of Pt and the emergence of the Nafion reflectance spectra were correlated to the onset of oxygen reduction catalysis. Oxygen reduction catalysis is coincident with the observance of a 2% step-increase in Pt reflectivity and the observance of the Nafion–Pt interface spectra initiating at 0.9 V and persisting down to the short circuit current.

Acknowledgments

Thanks are due to Army Research Office funding through grants W911NF-12-1-0346. This paper was presented at the ISPE-13 conference funded by ARO grant W911NF-12-1-0243.

REFERENCES

[1] Liu L, Pu C, Viswanathan B, Fan Q, Liu R, Smotkin ES. Carbon supported and unsupported Pt-Ru anodes for liquid feed direct methanol fuel cells. Electrochimica Acta 1998;43:3657–63.
[2] Liu L, Viswanathan R, Liu R, Smotkin ES. Methanol oxidation on Nafion spin-coated polycrystalline platinum and platinum alloys. Electrochemical and Solid-State Letters 1998;1:123–5.
[3] Ploense L, Salazar M, Gurau B, Smotkin ES. Proton spillover promoted isomerization of n-butylenes on Pd-black cathodes/Nafion 117. Journal of the American Chemical Society 1997;119:11550–1.
[4] Ploense L, Salazar M, Gurau B, Smotkin ES. Spectroscopic study of NEMCA promoted alkene isomerizations at PEM fuel cell Pd-Nafion cathodes. Solid State Ionics 2000;136–137:713–20.
[5] Salazar M, Smotkin ES. Electrochemically promoted olefin isomerization reactions at polymer electrolyte fuel cell membrane electrode assemblies. Journal of Applied Electrochemistry 2006;36:1237–40.
[6] Mosko JA. Automated determination of inorganic anions in water by ion chromatography. Analytical Chemistry 1984;56:629–33.
[7] Liu ST, Chen ZH, Xie JB, Lin JA, Chen ZJ, Rao PF. High-performance ion exchange chromatography of intact bacterial cells in the manner of molecules: 1. Establishment of methodology. Analytical Chemistry 2010;82:8544–50.
[8] Motoyama A, Xu T, Ruse CI, Wohlschlegel JA, Yates JR. Anion and cation mixed-bed ion exchange for enhanced multidimensional separations of peptides and phosphopeptides. Analytical Chemistry 2007;79:3623–34.
[9] Talwalkar S, Chauhan M, Aghalayam P, Qi ZW, Sundmacher K, Mahajani S. Kinetic studies on the dimerization of isobutene with ion-exchange resin in the presence of water as a selectivity enhancer. Industrial & Engineering Chemistry Research 2006;45:1312–23.
[10] Roman-Leshkov Y, Chheda JN, Dumesic JA. Phase modifiers promote efficient production of hydroxymethylfurfural from fructose. Science 2006;312:1933–7.
[11] Liu ZJ, Arnold RG, Betterton EA, Smotkin E. Reductive dehalogenation of gas-phase chlorinated solvents using a modified fuel cell. Environmental Science & Technology 2001;35:4320–6.
[12] Rubel F. Design manual: removal of arsenic from drinking water by ion exchange; 2003. Cincinnati, OH.
[13] Smotkin ES, Diaz-Morales RR. New electrocatalysts by combinatorial methods. Annual Review of Materials Research 2003;33:557–79.
[14] Syzdek JS, Armand MB, Falkowski P, Gizowska M, Karłowicz M, Łukaszuk Ł, et al. Reversed phase composite polymeric electrolytes based on poly(oxyethylene). Chemistry of Materials 2011;23:1785–97.
[15] Hassoun J, Croce F, Armand M, Scrosati B. Investigation of the O_2 electrochemistry in a polymer electrolyte solid-state cell. Angewandte Chemie International Edition 2011;50:2999–3002.
[16] Kim YT, Smotkin ES. The effect of plasticizers on transport and electrochemical properties of PEO-based electrolytes for lithium rechargeable batteries. Solid State Ionics 2002;149:29–37.
[17] Fernicola A, Weise FC, Greenbaum SG, Kagimoto J, Scrosati B, Soleto A. Lithium-ion-conducting electrolytes: from an ionic liquid to the polymer membrane. Journal of the Electrochemical Society 2009;156:A514–20.
[18] Topsoe H. Developments in operando studies and in situ characterization of heterogeneous catalysts. Journal of Catalysis 2003;216:155–64.

[19] Li J-T, Zhou Z-Y, Broadwell I, Sun S-G. In-situ infrared spectroscopic studies of electrochemical energy conversion and storage. Accounts of Chemical Research 2012;45:485–94.
[20] Shao MH, Warren J, Marinkovic NS, Faguy PW, Adzic RR. In situ ATR-SEIRAS study of electro oxidation of dimethyl ether on a Pt electrode in acid solutions. Electrochemistry Communications 2005;7:459–65.
[21] Pastor E, Wasmus S, Iwasita T, Arevalo MC, Gonzalez S, Arvia AJ. DEMS and in-situ FTIR investigations of C3 primary alcohols on platinum-electrodes in acid-solutions. Journal of Electroanalytical Chemistry 1993;353:81–100.
[22] Vigier F, Coutanceau C, Hahn F, Belgsir EM, Lamy C. On the mechanism of ethanol electro-oxidation on Pt and PtSn catalysts: electrochemical and in situ IR reflectance spectroscopy studies. Journal of Electroanalytical Chemistry 2004;563:81–9.
[23] Fan QB, Pu C, Lay KL, Smotkin ES. In situ FTIR-diffuse reflection spectroscopy of the anode surface in a direct methanol/oxygen fuel cell. Journal of The Electrochemical Society 1996;143:L21–3.
[24] Viswanathan R, Hou G, Liu R, Bare SR, Modica F, Mickelson G, et al. In-situ XANES of carbon-supported Pt-Ru anode electrocatalyst for reformate-air polymer electrolyte fuel cells. The Journal of Physical Chemistry B 2002;106:3458–65.
[25] Stoupin S, Chung E-H, Chattopadhyay S, Segre CU, Smotkin ES. Pt and Ru X-ray absorption spectroscopy of PtRu anode catalysts in operating direct methanol fuel cells. The Journal of Physical Chemistry B 2006;110:9932–8.
[26] Kendrick I, Kumari D, Yakaboski A, Dimakis N, Smotkin ES. Elucidating the ionomer-electrified metal interface. Journal of the American Chemical Society 2010;132:17611–6.
[27] Lewis EA, Kendrick I, Jia Q, Grice C, Segre CU, Smotkin ES. Operando X-ray absorption and infrared fuel cell spectroscopy. Electrochimica Acta 2011;56:8827–32.
[28] Evarts SE, Kendrick I, Wallstrom BL, Mion T, Abedi M, Dimakis N, et al. Ensemble site requirements for oxidative adsorption of methanol and ethanol on Pt membrane electrode assemblies. ACS Catalysis 2012;2:701–7.
[29] Wilson MS, Gottesfeld S. Thin-film catalyst layers for polymer electrolyte fuel-cell electrodes. Journal of Applied Electrochemistry 1992;22:1.
[30] Gurau B, Smotkin E. Methanol crossover in direct methanol fuel cells: a link between power and energy density. Journal of Power Sources 2002;112:339–52.
[31] Liu R, Iddir H, Fan Q, Hou G, Bo A, Ley KL, et al. Potential-dependent infrared absorption spectroscopy of adsorbed CO and X-ray photoelectron spectroscopy of arc-melted single-phase Pt, PtRu, PtOs, PtRuOs, and Ru electrodes. The Journal of Physical Chemistry B 2000;104:3518–31.
[32] Stamenkovic V, Chou KC, Somorjai GA, Ross PN, Markovic NM. Vibrational properties of CO at the Pt(111)-solution interface: the anomalous stark-tuning slope. The Journal of Physical Chemistry B 2005;109:678–80.
[33] Bo AL, Sanicharane S, Sompalli B, Fan QB, Gurau B, Liu RX, et al. In situ Stark effects with inverted bipolar peaks for adsorbed CO on Pt electrodes in 50 degrees C direct methanol fuel cells. The Journal of Physical Chemistry B 2000;104:7377–81.
[34] Sanicharane S, Bo A, Sompalli B, Gurau B, Smotkin ES. In situ 50 degC FTIR spectroscopy of Pt and PtRu direct methanol fuel cell membrane electrode assembly anodes. Journal of the Electrochemical Society 2002;149:A554–7.
[35] Blyholder G. Molecular orbital view of chemisorbed carbon monoxide. Journal of Physical Chemistry 1964;68:2772–8.
[36] Anderson AB, Kotz R, Yeager E. Theory for C-N- and AG-C vibrational frequency-dependence on potential – cyanide on a silver electrode. Chemical Physics Letters 1981;82:130–4.
[37] Ray NK, Anderson AB. Variations in C-O and Pt-C frequencies for CO on a platinum-electrode. Journal of Physical Chemistry 1982;86:4851–2.
[38] Hammer B, Morikawa Y, Nørskov JK. CO chemisorption at metal surfaces and overlayers. Physical Review Letters 1996;76:2141.
[39] Hammer B, Nielsen OH, Norskov JK. Structure sensitivity in adsorption: CO interaction with stepped and reconstructed Pt surfaces. Catalysis Letters 1997;46:31–5.
[40] Dimakis N, Iddir H, Diaz-Morales RR, Liu R, Bunker G, Chung E-H, et al. A band dispersion mechanism for Pt alloy compositional tuning of linear bound CO stretching frequencies. The Journal of Physical Chemistry B 2005;109:1839–48.
[41] Dimakis N, Navarro NE, Smotkin ES. Carbon monoxide adsorption on platinum-osmium and platinum-ruthenium-osmium mixed nanoparticles. Journal of Chemical Physics 2013;138.
[42] Dimakis N, Mion T, Smotkin ES. A density functional theory study on carbon monoxide adsorption on platinum-osmium and platinum-ruthenium-osmium alloys. Journal of Physical Chemistry C 2012;116:21447–58.
[43] Lewis EA, Segre CU, Smotkin ES. Embedded cluster Delta-XANES modeling of adsorption processes on Pt. Electrochimica Acta 2009;54:7181–5.
[44] Dimakis N, Cowan M, Hanson G, Smotkin ES. Attraction-repulsion mechanism for carbon monoxide adsorption on platinum and platinum-ruthenium alloys. Journal of Physical Chemistry C 2009;113:18730–9.
[45] Smotkin ES. Chapter 8 – FTIR and X-ray absorption spectroscopy of operating fuel cells. In: Shi-Gang S, Paul Andrew C, Andrzej Wieckowski, editors. In-situ spectroscopic studies of adsorption at the electrode and electrocatalysis. Amsterdam: Elsevier Science B.V.; 2007. p. 247–72.
[46] Persson BNJ, Ryberg R. Vibrational interaction between molecules adsorbed on a metal-surface – the dipole-dipole interaction. Physical Review B 1981;24:6954–70.
[47] Silverstein RM, Bassler GC, Morrill TC. Spectrometric identification of organic compounds. 5th ed. Wiley; 1991.
[48] Webber M, Dimakis N, Kumari D, Fucillo M, Smotkin ES. Mechanically coupled internal coordinates of ionomer vibrational modes. Macromolecules 2010;43:5500–2.
[49] Kendrick I, Yakaboski A, Kingston E, Doan J, Dimakis N, Smotkin ES. Theoretical and experimental infrared spectra of hydrated and dehydrated nafion. Journal of Polymer Science Part B: Polymer Physics 2013;51:1329–34.